

EXPERIMENT AND ANALYSIS ON THE CREEP-FATIGUE DAMAGE OF A 316SS NONLINEAR STRUCTURE IN LIQUID METAL REACTOR SUBJECTED TO A CYCLIC LOADING WITH 1HR HOLD TIME

J.B. Kim, H.Y. Lee, C.G. Park, and J.H. Lee
Korea Atomic Energy Research Institute, Korea
150 Dukjin-dong, Yuseong-gu, Daejeon 305-353, South Korea
E-mail: jbkim@kaeri.re.kr

ABSTRACT

The high temperature environment of the Liquid Metal Reactor (LMR) may cause the creep-fatigue damage in the reactor structures and it is important to be dealt with from a structural integrity point of view. This paper deals with the creep-fatigue damage evaluation of a typical geometrical discontinuity structure made of 316SS subjected to both a tensile loading and a high temperature loading. The creep-fatigue structural test of a cylindrical structure welded with a conical shell has been carried out with a 1MN IST actuator and a 50kW induction heater with 1 hour hold time at 550°C. Total 400 cycles of testing were performed and the creep-fatigue damage in the discontinuous regions and the defect front, which were prepared by an electric discharge machining, were investigated using nondestructive methods. Also, the high temperature structural analysis program (NONSTA-VP) implementing Chaboche's unified viscoplasticity model into ABAQUS, developed to analyze creep-fatigue behavior, has been used to evaluate the creep-fatigue damage and the result has been compared with those of the structural test. The creep-fatigue crack initiation and growth behavior at the defect front were assessed and compared with the test results.

Keywords: Creep, Fatigue, Damage, Crack Initiation, Crack Growth

1. INTRODUCTION

The 600MWe Liquid Metal Reactor KALIMER-600[1] has been under development in Korea and the operating temperature is 545°C. Therefore the high temperature reactor structures may exhibit a highly nonlinear elastoplastic deformation behavior such as ratcheting and the time dependent creep deformation during the high temperature operation periods. This creep behavior of the structure induces difficulties in the assessment of a high temperature structural integrity. The creep-fatigue damage is one of the principal concerns to be dealt with for its structural integrity. Low cycle fatigue damage due to a thermal transient loading interacts with the creep damage during a high temperature hold time and this interaction reduces the life of the high temperature structures. The high temperature structure design guidelines such as BDS[2], RCC-MR[3], and ASME-NH[4] depend mainly upon the elastic approach with conservatism. Even though these guidelines allow one to use a detailed inelastic analysis method, they do not provide the proper inelastic constitutive equations. Thus a systematic analysis technology utilizing an inelastic analysis, accounting for both the time independent plasticity and the time dependent creep behaviors for a reliable structural safety assessment is necessary.

In this study, the several inelastic constitutive models proposed by Perzyna[5], Phillips and Wu[6], Robinson[7], Chaboche[8-10], Bodner and Partom[11], and Miller[12], respectively were reviewed. Among them, the Chaboche's viscoplasticity constitutive equation was selected and implemented into a general purpose finite element code ABAQUS as a subroutine NONSTA-VP[13] since it was considered as the most promising

model to simulate both the time independent elastoplastic behavior and the time dependent creep behavior. As part of the validation efforts, a uniaxial analysis had already been compared with test results[13] and a creep-fatigue structure test with a Y-junction structure of a 7mm thickness had been carried out. The interim damage observation with 100 cycles of a structural test was compared to the analysis results[14]. In this study, another creep-fatigue structure test was performed with a 5mm thick cylindrical specimen representing a typical nonlinear structure in KALIMER-600 shown in Fig.1. In the test model, both the surface defects and the penetrating defects were machined and the creep-fatigue damage developments ahead of the defects as well as around the geometrical nonlinear region were investigated. In the fiscal year of 2004, a total of 400 cycles of a creep-fatigue structure test were performed and the corresponding creep-fatigue damage assessment was carried out.

Both the elastic analysis and the inelastic analysis using the NONSTA-VP code were performed with the collected temperature profiles from the test. The strain results of the analyses and the damage evaluations were compared with the test results.

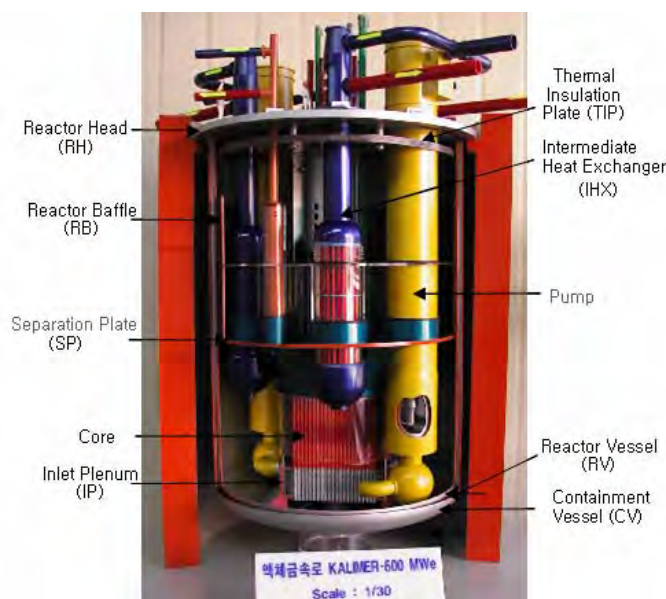


Fig. 1 KALIMER-600 Reactor Structures



Fig.2 Creep-fatigue Test Facility

2. CREEP-FATIGUE STRUCTURE TEST

The creep-fatigue test facility is composed of a 1MN hydraulic actuator, load frame and an anchored base plate as shown in Fig.2. Heating unit applying the thermal load is a high frequency induction heater of which the capacity is 50kHz and 50kW. Fig.2 shows 6 turns of the copper heating coil surrounding the structural model used to apply the heat to the center zone of the test model.

Axial tensile load was applied by the IST 1MN hydraulic actuator by simulating the dead weight of the reactor structures and the thermal load was applied by a high frequency induction heater simulating the startup-hold-shutdown condition. The load and displacement data was collected continuously by a Labtronic-8800 controller. Vertical strain was measured by the high temperature extensometer (Instron Model 2632) and the radial displacement was measured by the LVDT(Schaevitz Model CA-121-200). The filament type high temperature strain gages developed by the Measurement Group (Model C-020708-D) were installed by a spot welding along both the longitudinal direction and the circumferential direction to measure the strains directly.

To acquire and control the temperature of the test model, 24 channels of the K-type thermocouple were spot welded onto the inner surface of the test model along the axial direction, 10 channels were welded onto the outer surface in the axial direction, 6 channels were welded onto the inner skirt, and 3 channels were welded along the circumferential direction.

The creep-fatigue structural test model is a geometrically nonlinear structure of which the shape is a cylinder and a cone type skirt is attached to the inside surface of the cylinder at a center location by TIG welding as

shown in Fig. 3. The Type 316 stainless steel is used for the test model and the thickness, outer diameter, and height of the test model are 5mm, 600mm and 500mm, respectively. The thickness and length of the cone structure are 5mm and 200mm, respectively. And 4 defects were prepared by an electric discharge machining arranged at 90 degree intervals along the circumferential direction to obtain the accelerated damage development ahead of the defect front. Two of them are through wall defects, 20mm in length and 0.25mm in corner radius each, and arranged in the vertical direction and circumferential direction, respectively. Another two defects are elliptic shaped surface defects, 20mm in length and 1.25mm in depth, and arranged in the vertical direction and circumferential direction, respectively.

Tensile load was increased to 500kN for 10 seconds, maintained for 1 hour, and removed. Load control was accomplished by Labtronic 8800. At the same time, the thermal load was applied to the center region of the test model as shown in Fig.4 using a high frequency induction heater. . It took 5 minutes for the temperature of the test model to reach 550°C. Thermal load was controlled to maintain the temperature of the test model at 550°C for one hour and then removed. One cycle of loading took 95minutes and a total of 400 cycles of testing were carried out.

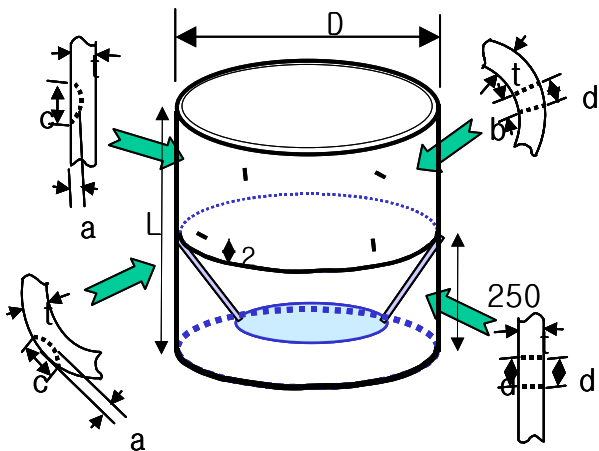


Fig. 3 Creep-fatigue Test Model

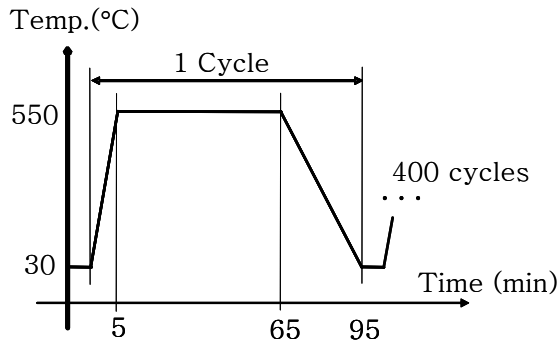


Fig.4 Creep-fatigue Temperature Loading

3. DAMAGE INSPECTION AND TEST RESULTS

The interim field inspection was scheduled for every 100th cycle of the testing. A nondestructive metallurgical inspection was performed on the spot. A portable optical zoom microscope, shown in Fig.5, was used to investigate the creep-fatigue damage on the test model with the maximum magnification ratio of 3500 times. Several inspection points on the test model were ground, polished, and etched according to the standard procedure[15]. To supplement the optical observation results, a replica technique was utilized on the spot. After a surface treatment, several spots of interest were carefully replicated. The scanning electron microscope (SEM) was used to investigate the creep-fatigue damage evolution as shown in Fig.6.



Fig. 5 Surface Examination (DZ2)



Fig.6 Scanning Electron Microscope (JEOL)

Figure 7 and Fig.8 show the interior geometrically nonlinear region where the cone structure was welded to the inside of the cylinder model after 100 cycles and 400 cycles, respectively, magnified 2200 times and the apparent creep-fatigue damage is hardly observed along the grain boundaries.

Figure 9 and Fig.10 show the vicinity of the vertical through wall defect of the test model after 100 cycles and 400 cycles, respectively, magnified 350 times. The creep-fatigue damage occurred and formed microcracks along the grain boundaries emanating from the edge of the defect front.

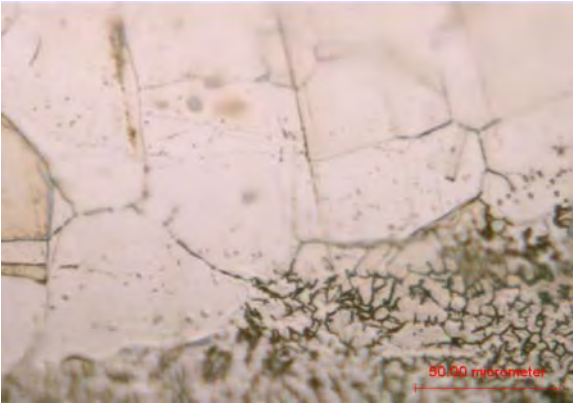


Fig.7 Interior Nonlinear Region (100cycles, X2200)

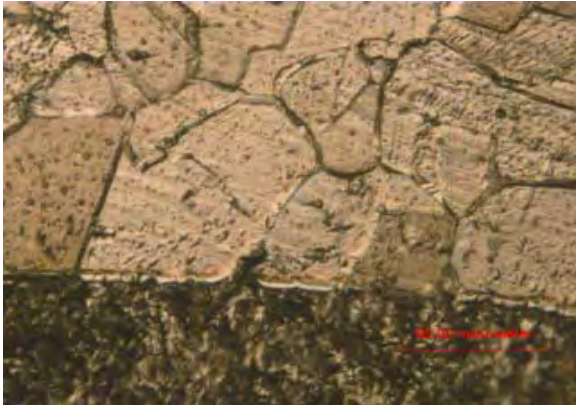


Fig.8 Interior Nonlinear Region (400cycles, X2200)

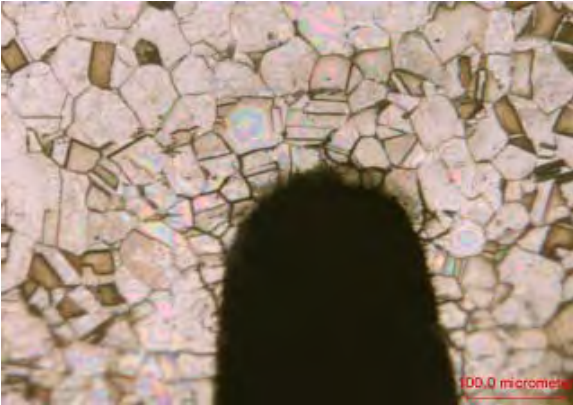


Fig.9 Vertical Defect Front (100cycles, X350)

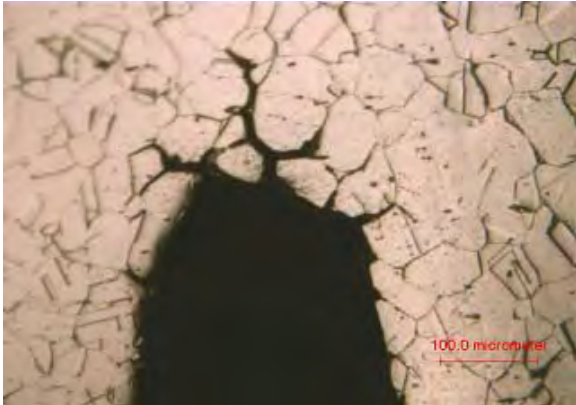


Fig.10 Vertical Defect Front (400cycles, X350)

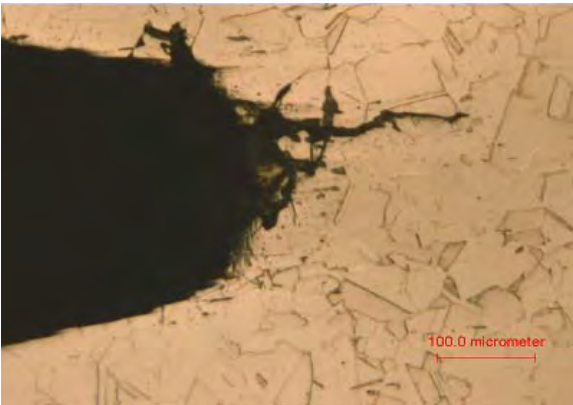


Fig.11 Horizontal Defect Front (300cycles, X350)

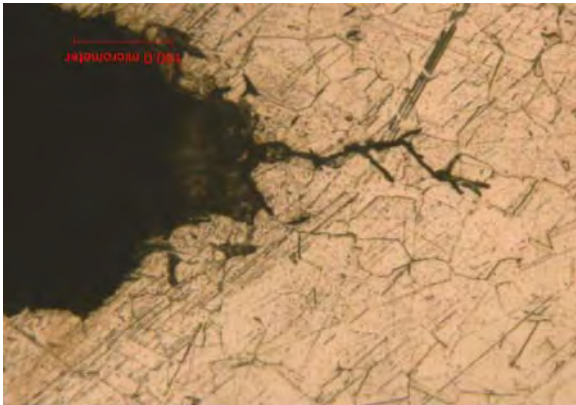


Fig.12 Horizontal Defect Front (400cycles, X350)

Figure 11 and Fig.12 show the vicinity of the horizontal through wall defect of the test model after 300 cycles and 400 cycles, respectively, magnified 350 times. The creep-fatigue damage occurred along the grain boundaries emanating from the edge of the defect front and had grown into a microcrack of which the size was approximately 0.32mm. Figure 13 and Fig.14 show the vicinity of the defect front observed by the SEM after 100 cycles and 400 cycles, magnified 2000 times, respectively. The surface was replicated on the spot for convenient observation using the SEM. After 400 cycles of a testing, it is clearly seen that the precipitations were produced along the grain boundaries due to the creep-fatigue damage.

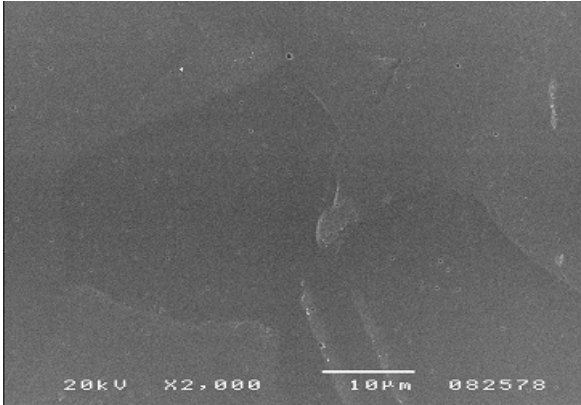


Fig.13 Horizontal Defect Front (100cycles, X2000)

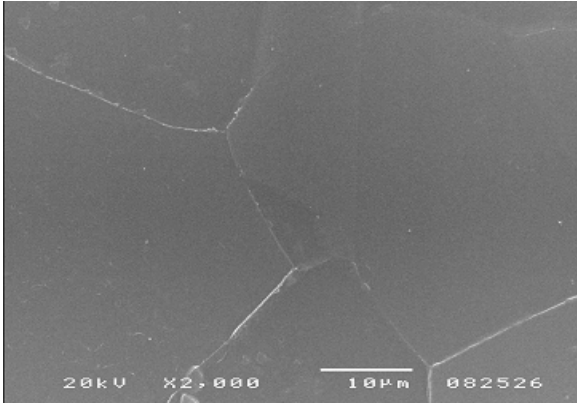


Fig.14 Horizontal Defect Front (400cycles, X2000)

It is considered that the test time of 400 cycles is not yet ripe for the generation of the creep-fatigue damage in the test model other than the defect regions as shown in Fig.7 and Fig.8. In the vicinity of the defect front, the creep-fatigue occurred and formed microcracks since the stress values around the defect front were large enough to generate the creep-fatigue damage with a given amount of testing cycles as shown in Fig.9 ~ Fig.14. Another point of interest is the observation of the growth behavior of the microcracks initiated after a certain number of testing cycles. With 400 cycles of a testing, microcracks seemed to grow at a constant speed but it is premature to derive a conclusion regarding the crack growth behavior in this test model at this time. It is necessary to perform further cycles of a testing to examine the growth behavior of microcracks into macrocracks.

4. CREEP-FATIGUE STRUCTURAL EVALUATION AND COMPARISONS

The creep-fatigue damage evaluations based upon both the elastic analysis method and the detailed inelastic analysis method were performed by applying the temperature profiles of the test model obtained during the creep-fatigue test, and the analysis results were compared with those from the test.

For the finite element analysis using ABAQUS/CAE6.3[16], axisymmetric 6-node 64 triangular elements and 8-node 334 quadrilateral elements with a total of 1501 nodes were used as shown in Fig.15. DCAX6/DCAX8 elements were used for the thermal analysis and CAX6/CAX8 elements were used for the stress analysis. As a boundary condition the top and bottom surfaces were constrained in the radial direction. The tensile load a 500kN was applied to the top surface according to the load sequence as in the test procedure. Temperature distribution in the Y-junction structure from the thermal analysis by applying the temperature profiles along the inner and outer surfaces is transferred to the stress analysis to calculate the thermal stresses. Thermal properties and mechanical properties of the 316SS are shown in Table 1 and Table 2[17].

Table 1 Thermal Properties of 316SS

Temperature(°C)	Conductivity(J/s.m. °C)	Density(kg/m ³)	Specific Heat(J/kg. °C)
37.78	13.656	7962	472.33
148.9	15.520	7908	509.70
260.0	17.319	7864	536.68
371.1	19.051	7814	556.16

482.2	20.716	7767	571.03
537.8	21.522	7739	577.64
593.3	22.311	7717	584.18

Table 2 Mechanical Properties of 316SS

Temperature(°C)	Young's Modulus(GPa)	Poisson's Ratio	Thermal Expansion(x10 ⁻⁶)
37.78	192	0.3	15.9
100.0	186	0.3	16.4
200.0	178	0.3	17.0
300.0	170	0.3	17.5
400.0	161	0.3	17.9
500.0	153	0.3	18.3
600.0	145	0.3	18.7

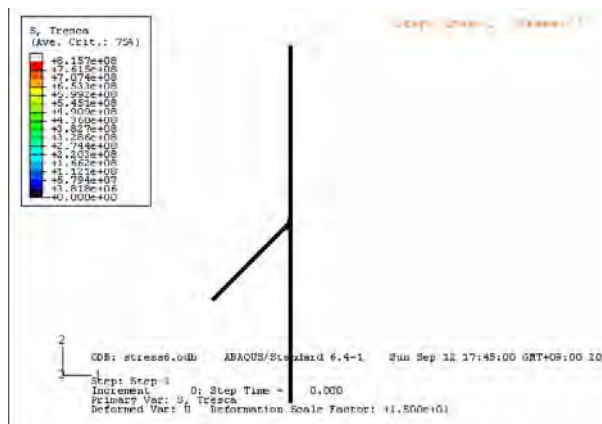


Fig.15 Finite Element Analysis Model

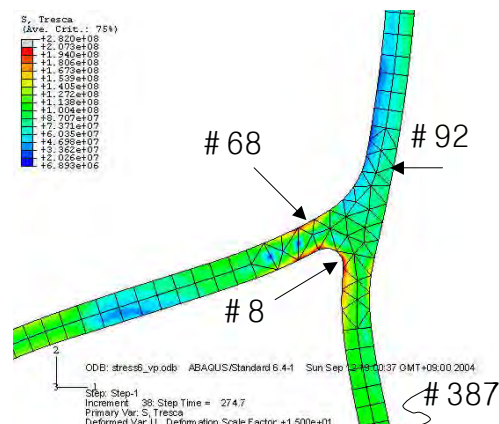


Fig.16 Stress Intensity Distribution (550°C)

In this study both the elastic analysis and detailed inelastic analysis were used for the comparison. Elastic analysis itself cannot trace the real behavior of the structure but one can predict its inelastic behavior per the ASME-NH procedure by employing the elastic analysis result with a conservatism.

The unified viscoplasticity constitutive model such as the Chaboche model is well known to exhibit an excellent prediction of both the plasticities. In this study, a Chaboche's unified viscoplasticity model was implemented into ABAQUS as a UMAT subroutine (NONSTA-VP) to perform the nonlinear structural analysis. The constitutive equations are as follows:

Stress-strain relationship can be defined as

$$\dot{\sigma} = E(\dot{\epsilon} - \dot{\epsilon}_p) = E \left\{ \dot{\epsilon} - \frac{3}{2} \left\langle \frac{J(\mathbf{s} - \mathbf{X}) - (R + \kappa)}{K} \right\rangle^n \frac{\mathbf{s} - \mathbf{X}}{J(\mathbf{s} - \mathbf{X})} \right\} \quad (1)$$

Viscoplastic strain rate ($\dot{\epsilon}_p$) and accumulated plastic strain rate (\dot{p}) are

$$\dot{\epsilon}_p = \dot{p} \mathbf{n}, \quad \dot{p} = \left\langle \frac{J(\mathbf{s} - \mathbf{X}) - (R + \kappa)}{K} \right\rangle^n \quad (2)$$

where $\mathbf{n} = \frac{3}{2} \frac{\mathbf{s} - \mathbf{X}}{J(\mathbf{s} - \mathbf{X})}$.

Kinematic hardening and isotropic hardening evolutions are defined as

$$\dot{X} = \frac{2}{3} C \dot{\epsilon}_p - \gamma \dot{X} \dot{p} = \left(\frac{2}{3} C \mathbf{n} - \gamma \dot{X} \right) \dot{p} \quad (3)$$

$$\dot{R} = b(Q - R) \dot{p} \quad (4)$$

where C and γ describe the amount of kinematic hardening, Q and b describe the cyclic hardening, and κ is the constant indicating the initial yield. It is noted that κ is different from the conventional yield stress since there is no yield concept in the viscoplasticity theory. X is the back stress, R is the drag stress (change in the size of

elastic domain), p is the accumulated plastic strain, and function $\langle x \rangle$ is defined as: $\langle x \rangle = x$ if $x \geq 0$, $\langle x \rangle = 0$ if $x < 0$.

Inelastic material constants for the NONSTA-VP are shown in Table 3[9].

Table 3 NONSTA-VP parameters for 316SS

E	149.6GPa	ν	0.309	α	19.7×10^{-6}	κ	6MPa
C	24800MPa	γ	300	b	10	Q	80MPa
K	150MPa	n	12				

Figure 16 shows the stress intensity distribution in the junction region just after the heating zone reaches 550°C. Node 387 indicates the location for the measurement using the extensometer, strain gage, and the LVDT. Node 8 and node 68 are expected to be the area of a stress concentration. Thermal shock effect turned out to be small due to the low cooling rate 0.3°C/s when compared to the heating rate 1.8°C/s. The characteristics of the axial stress are a small membrane stress and a large bending stress and the characteristics of the circumferential stress are a large membrane stress and a small bending stress.

The axial and circumferential deformations obtained by the analysis agree with the test results to within a 10% difference. Maximum elastic strain range at node 68 calculated per ASME NH is 0.17%. Applying this to a design fatigue curve yields allowable cycles of 31,200 and the fatigue damage for 400 cycles by the ASME-NH procedure is evaluated by equation (5).

$$D_f = \sum_{j=1}^p \left(\frac{n}{N_d} \right)_j = \frac{400}{31200} = 0.013 \quad (5)$$

In addition, the stress level for the creep damage evaluation is calculated as $\frac{S_r}{K} = \frac{163}{0.67} = 245$ (MPa) and the allowable time duration is 6,500 hours with a creep rupture curve. Creep damage following ASME-NH for 400 cycles of a loading is evaluated by equation (6).

$$D_c = \sum_{k=1}^q \left(\frac{\Delta t}{T_d} \right)_k = \frac{400}{6500} = 0.062 \quad (6)$$

The above creep-fatigue damage was assessed by equation (7) and is indicated in the creep-fatigue damage interaction diagram, Fig.17, and it can be seen that a small amount of damage agrees with the test result.

$$D_f + D_c = \sum_{j=1}^p \left(\frac{n}{N_d} \right)_j + \sum_{k=1}^q \left(\frac{\Delta t}{T_d} \right)_k \quad (7)$$

In addition, a detailed inelastic analysis using NONSTA-VP was performed and the creep-fatigue damage according to the ASME-NH procedure was evaluated. The advantage of the inelastic approach is its simplicity because it is not necessary to follow a complex procedure which is required for the case of the elastic approach to estimate the real structure inelastic behavior. With the stresses and strains from the detailed inelastic analysis, the creep-fatigue damage can be assessed in a direct manner. Maximum strain range by the inelastic analysis is 0.001 at node 68 and an application to the ASME-NH yields a fatigue damage of 0.001. To evaluate the creep damage, the equivalent stress was calculated by equation (8).

$$\sigma_e = \bar{\sigma} e^{\left[c \left(\frac{J_1}{S_s} - 1 \right) \right]} \quad (8)$$

where $J_1 = \sigma_1 + \sigma_2 + \sigma_3$, $S_s = \sqrt{\sigma_1^2 + \sigma_2^2 + \sigma_3^2}$

$$\bar{\sigma} = \frac{1}{\sqrt{2}} \sqrt{(\sigma_1 - \sigma_2)^2 + (\sigma_2 - \sigma_3)^2 + (\sigma_3 - \sigma_1)^2}$$

The equivalent stress histories were segmented by several flat regions and the creep damage was calculated for each region. Linear summation of each creep damage leads to a total creep damage and it is 0.0013 at node 68. Creep-fatigue damage assessed by the inelastic approach is shown in Fig.17 and it can be concluded that the creep-fatigue damage for 400 cycles is very small as in the case of the elastic approach. The required number of test cycles to have an apparent creep-fatigue damage in the test model other than the defect region based upon the elastic approach is 4,000 and the one based upon the detailed inelastic analysis is 100,000. While it is premature to jump to a conclusion from the comparison of 400 cycles of the testing results and the analysis results, the creep-fatigue damage assessment near the defect region was carried out and compared with the test results.

Among the evaluation methods of the defect growth initiation evaluation methods, the UK R5/R6 code, Japanese JNC method, and the French RCC-MR A16 have been presented recently. In this study, the RCC-MR A16 procedure is applied to evaluate the crack initiation and growth of a cylindrical structure with a circumferential through wall defect[18].

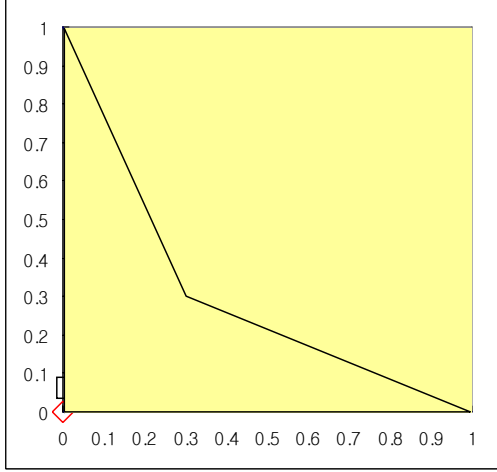


Fig.17 Creep-fatigue Damage Envelop

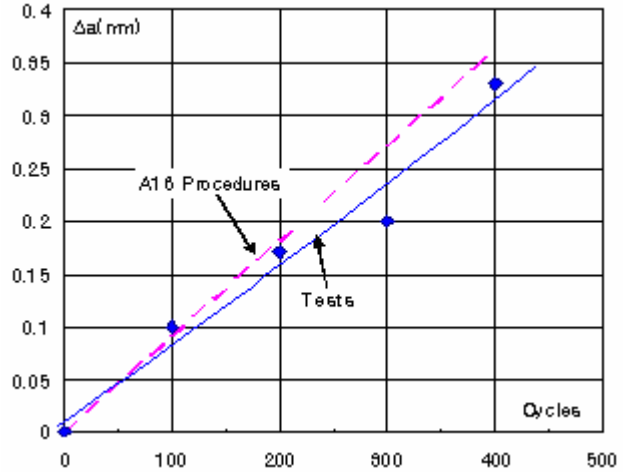


Fig.18 Crack Growth Comparison

Creep-fatigue crack initiation is assessed based on the σ_d method[19]. The principle of this method is to determine a stress and a strain at a characteristic distance from the crack tip and to compare them with material fatigue and creep data. A characteristic distance is 0.05mm for 316SS[3]. To calculate the elastic stress range $\Delta\sigma_{de}$ in an evaluation model, FE analysis is carried out using ANSYS 9.0 software[20]. From the FE analysis result, $\Delta\sigma_{de}$ is 819.4MPa at the crack front at distance d and the strain range due to a plasticity $(\Delta\varepsilon)_{el+pl}$ is 1.059(%). Allowable cycle for this value is 241 and the fatigue usage fraction is determined by $A=n/241$. Creep usage fraction is determined from the creep rupture time and the creep rupture time is determined from the $\Delta\sigma_{kd}$ estimated as 319MPa. The creep rupture time T on the S_r curve corresponding to 550°C and $\Delta\sigma_{kd}$ is 125 hours. Therefore the creep usage fraction is determined by $W=t/125$. With these results, it is concluded that a creep-fatigue crack would initiate in 57 cycles and 57 hours of a high temperature hold time. This agrees well with the observation results.

The creep-fatigue crack growth was evaluated with the determination of the fracture mechanic parameters J and $C^*(t)$ for a mechanical loading and a thermal gradient. Creep-fatigue crack growth is calculated by a linear summation of the fatigue crack growth and the creep crack growth during the hold time. The fatigue crack growth was evaluated by equation (9).

$$J_s = \left[\sqrt{J_{el}^{me}} + \frac{\sigma^{me+th}}{\sigma_{el}^{me+th}} \cdot \sqrt{J_{el}^{th}} \right]^2 \cdot \frac{E \cdot \varepsilon_{ref}^{me+th}}{\sigma_{ref}^{me+th}}, \quad \frac{da}{dN_f} = 3.095 \times 10^{-4} [mm / cycle] \quad (9)$$

The creep crack growth was evaluated by equation (10).

$$C_s^*(t) = \left[\sqrt{J_{el}^{me}} + \frac{\sigma^{me+th}(t)}{\sigma_{el}^{me+th}} \cdot \sqrt{J_{el}^{th}} \right]^2 \cdot \frac{E \cdot \dot{\varepsilon}_{ref}^{me+th}(t)}{\sigma_{ref}^{me+th}(t)} \quad \frac{da}{dt_c} = 6.01 \times 10^{-4} [mm / hr] \quad (10)$$

The creep-fatigue crack growth after 400 cycles of a testing was 0.36mm and this slightly overestimates the test results as shown in Fig.18. Even though a good agreement between the analysis and the test results was obtained with 400 cycles, it is necessary to perform more cycles of testing to deduce final conclusion. After 800 or 1000 cycles of a testing, it is expected that the propagated crack may be regarded as a macrocrack and we can investigate the crack growth behavior of both a microcrack and a macrocrack.

5. CONCLUSIONS

In this study, the creep-fatigue structural test of a 316SS Y-junction cylinder was carried out and results were compared with those by both the elastic analysis and detailed inelastic analysis using the developed NONSTA-VP. After 400 cycles of a testing, creep-fatigue damage is hardly observed in the test model other than

the defect region. In the test model, penetrated defects and surface defects were prepared to investigate the damage development ahead of the defects. After 400 cycles of a creep-fatigue loading were applied, the corresponding creep-fatigue crack initiated and grew to 0.33mm. Both the elastic analysis and inelastic analysis using the NONSTA-VP code were performed with the collected temperature profiles from the test and the strain results of the analyses agreed well with those from the test. The creep-fatigue damage was assessed per ASME-NH by utilizing the analysis results and a very small amount of damage was obtained of which the result coincided with the test result. The creep-fatigue crack initiation and growth evaluation for a cylindrical structure with a circumferential through wall defect was carried out according to the RCC-MR A16 defect assessment guide. The evaluation result for the model shows that a creep-fatigue crack was initiated after about 57 cycles and this agrees well with the test result. The creep-fatigue crack growth was evaluated with the determination of the fracture mechanic parameters J and $C^*(t)$ for a mechanical loading and a thermal gradient. Also, an experimental test was performed to compare it with the evaluation result. The observed result shows that the values of the crack growth evaluation are close to the experimental results by maintaining a conservatism.

ACKNOWLEDGMENTS This Work was supported by the Korean Ministry of Science and Technology through its National Nuclear Technology Program.

REFERENCES

- [1] D.H. Hahn, (2000), KALIMER Conceptual Design Report, KAERI/TR-2204, Korea Atomic Energy Research Institute, Daejeon.
- [2] PNC, (1984), Structural Design Guide for Class 1 Components of Prototype Fast Breeder Reactor for Elevated Temperature Service, Japan.
- [3] AFCEN, (2002), Design and Construction Rules for Mechanical Components of FBR Nuclear Islands, RCC-MR, 2002 Edition.
- [4] ASME, (2004), ASME Boiler and Pressure Vessel Code, Section III, Rules for Construction of Nuclear Power Plant Components, Div. 1, Subsection NH, Class 1 Components in Elevated Temperature Service.
- [5] P. Perzyna, (1963), "The Constitutive Equations for Rate Sensitive Plastic Materials," Quarterly Appl. Math., Vol. 20, p. 321.
- [6] A. Phillips and H. C. Wu, (1973), "A Theory of Viscoplasticity," Int. J. Solids and Struc., Vol. 9, p. 15.
- [7] D. N. Robinson, (1978), "A Unified Creep-Plasticity Model for Structural Metals at High Temperatures," ORNL/TM 5969.
- [8] J. L. Chaboche and G. Rousselier, (1983), "On the Plastic and Viscoplastic Constitutive Equations - Part 1 : Rules developed with internal variable concept," J. of Press. Vess. Tech., Vol. 15, p. 153.
- [9] J. L. Chaboche, (1990), Mechanics of Solid Materials, Cambridge University Press.
- [10] J. L. Chaboche, (1993), "Cyclic Viscoplastic Constitutive Equations, Part I : A Thermodynamically Consistent Formulation," J. Appl. Mech., Vol. 60, p. 813.
- [11] S. R. Bodner and Y. Partom, (1975), "Constitutive Equations for Elasto-Viscoplastic Strain Hardening Materials." J. Appl. Mech., Vol. 42, p. 235.
- [12] A. K. Miller, (1976), "An Inelastic Constitutive Model for Monotonic, Cyclic and Creep Deformation: Part 1, Equations, Development and Analytical Procedures and Part 2, Application to type 304 stainless steel," J. Engng. Mat. and Tech., Vol. 98, p. 97.
- [13] J.B. Kim, (1999), Development of NONSTA Code for the Design and Analysis of LMR High Temperature Structures, KAERI/TR-1256.
- [14] J.B.Kim, H.Y.Lee, C.G.Park, G.P.Jeon, J.H.Lee, (2004), "Creep-Fatigue Damage Evaluation of the 316SS Y-junction Structures in a Liquid Metal Reactor," Proceedings of ICAPP '04, Paper4323, Pittsburgh, PA USA.
- [15] J.S. Park, (2000), "Standard Procedure of Replication for High Temperature Equipment Life Estimation," Proc. of KSME, Vol. A, No.24, 9, pp.2381-2386.
- [16] HKS, (2002), ABAQUS Users manual, Version 6.2, USA.
- [17] S.S.Youn, S.B. Lee, J.B. Kim, H.Y. Lee, and B.Yoo, (1998), "Implementation of Thermoviscoplastic Constitutive Equations into the Finite Element Code ABAQUS," Proc. of the KNS, Oct.
- [18] C.G.Park, J.B.Kim, H.Y.Lee, Y.S.Ju, and J.H.Lee, (2005), "Creep-Fatigue Crack Initiation and Growth Behavior at the Defect Front of 316SS Cylindrical Structure in a Liquid Metal Reactor," Proceedings of ICAPP '05, Paper5232, Seoul, Korea.
- [19] B. Drubay, S. Marie, S. Chapuliot, M.H. Lacire, B. Michel, H. Deschanel, (2003), "A16: Guide for Defect Assessment at Elevated Temperature," International Journal of Pressure Vessels and Piping, Vol.80, p.499-516.
- [20] Swanson Analysis System, Inc., (2004), ANSYS user manual for version 9.0.